Supporting Information

Embedding covalency into metal catalysts for efficient electrochemical conversion of CO_2

Hyung-Kyu Lim[§,†], Hyeyoung Shin[§,†], William A. Goddard III[‡], Yun Jeong Hwang[‖], Byoung Koun Min[‖], and Hyungjun Kim[†,*]

[†] Graduate School of Energy, Environment, Water, and Sustainability (EEWS), Korea Advanced Institute of Science and Technology (KAIST), Yuseong-gu, Daejeon 305-701, Korea

[‡] Materials and Process Simulation Center, Beckman Institute, California Institute of Technology, Pasadena, CA 91125, U.S.A

[‖] Clean Energy Research Center, Korea Institute of Science and Technology (KIST), Seongbuk-gu, Seoul, 136-791, Korea

[*] Corresponding author. Email: linus16@kaist.ac.kr

[§] These authors contributed equally to this work.

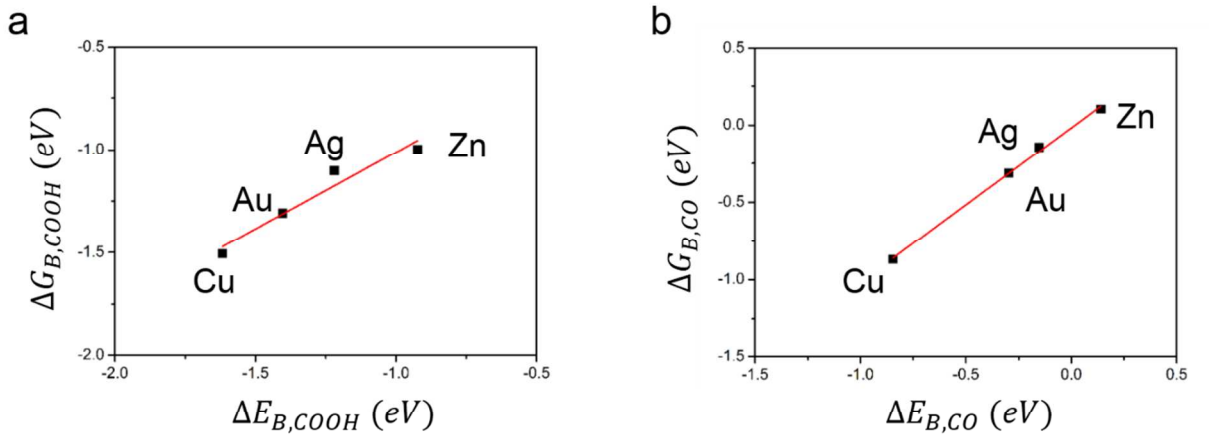

$$\Delta G_{B,COOH} = 0.7444 \times \Delta E_{B,COOH} - 0.2679 \qquad R^2 = 0.918$$

$$\Delta G_{B,CO} = 0.9959 \times \Delta E_{B,CO} - 0.0183 \qquad R^2 = 0.997$$

Figure S1. The correlation between the binding enthalpy and the solvated binding free energy for (**a**) ·COOH radical and (**b**) CO.

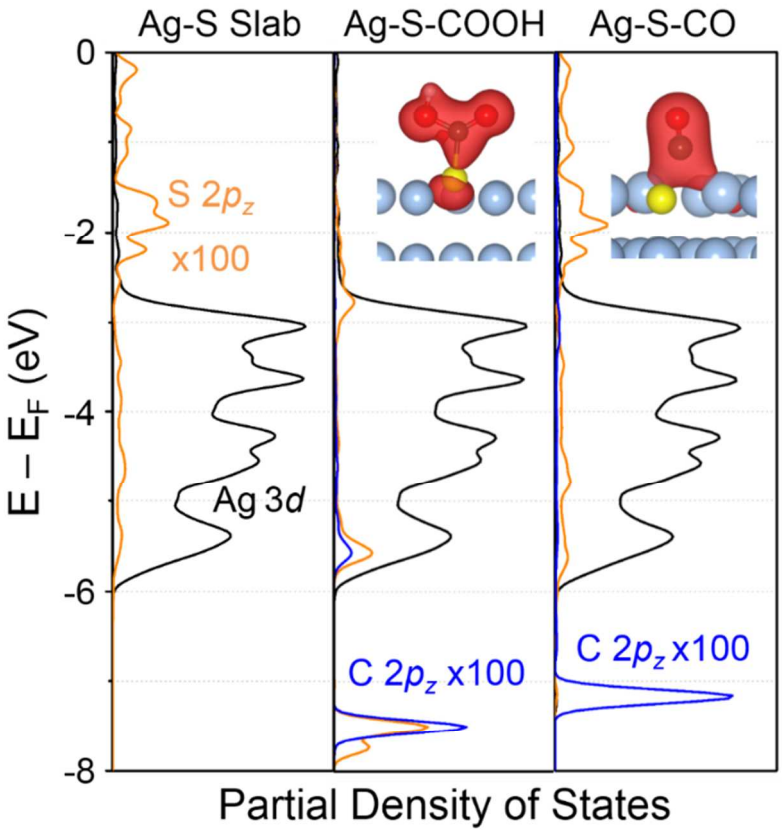

Figure S2. The partial density of states analysis for the Ag-S, AgS-COOH, and AgS-CO systems, and the corresponding electron-density plot for which the $2p_z$ orbital of C exists.

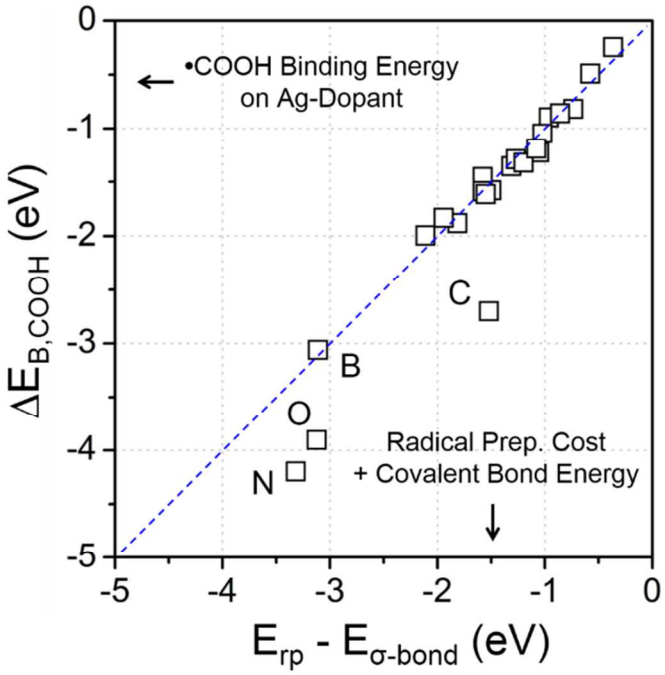

Figure S3. The comparison between the ·COOH binding enthalpy on doped silver and the estimated value from the summation of the radical-preparation cost and the binding energy for ·COOH.

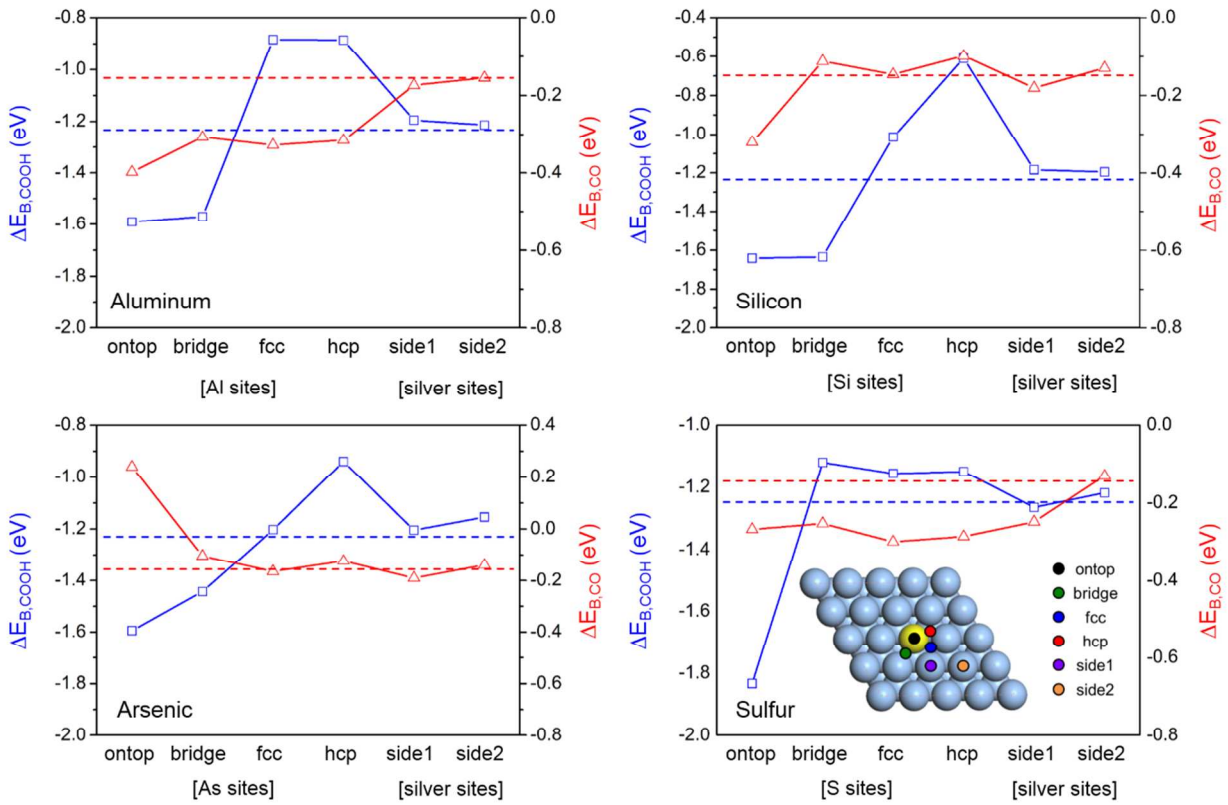

Figure S4. The ·COOH and CO binding enthalpy trend in terms of the sites around a sulfur dopant. The strongest binding site is the on-top site for ·COOH and the FCC site for CO.

Table S1. The overall quantum-mechanical energetics and the experimental reduction potential for electrochemical CO_2 reduction to CO with or without a catalyst. The experimental reduction potential for copper (denoted with *) originates from the third reduction process (**Table S2**).

(eV)	**No-cat.**	**Zn**	**Ag**	**Au**	**Cu**
$\Delta G_{B,\cdot COOH}$	-	-1.00	-1.10	-1.31	-1.51
$\Delta G_{B,CO}$	-	0.10	-0.15	-0.31	-0.87
Γ_1	2.02	1.02	0.91	0.71	0.51
Γ_2	-1.07	0.03	-0.11	-0.07	-0.43
$E°_{Theory}$ **(vs. SHE)**	-2.02	-1.02	-0.91	-0.71	-0.51(*-0.97)
$E°_{Experimental}$ **(vs. SHE)**	-	-1.12	-0.95	-0.72	-1.02
Γ_3	-0.50	-0.61	-0.36	-0.19	0.37

* $E°_{Theory} = -MAX(\Gamma_1, \Gamma_2)$

Table S2. The theoretical reduction potential for the further reduction process on copper surface. Both the overpotential for ·COH and ·CHO result in the same value.

(eV)	No-cat.	Cu
$\Delta G_{B,CO}$	-	-0.87
$\Delta G_{B,\cdot COH}$	-	-2.65
$\Delta G_{B,\cdot CHO}$	-	-1.12
Γ_3	2.75	0.97
Γ_4	1.22	0.97
$-MAX(\Gamma_3, \Gamma_4)$	-2.75	-0.97
$E°_{Experimental}$ (vs. SHE)	-	-1.02

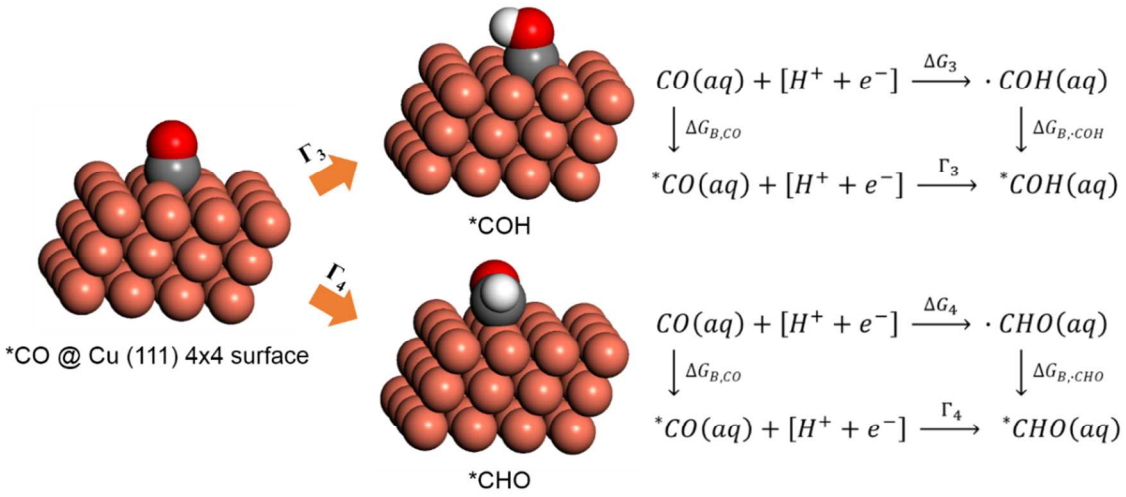

Table S3. The electronegativity and the Bader charge of the major *p*-block dopants. All dopants are negatively charged, implying that the *p*-orbitals are overfilled compared to in the neutral atomic state.

***p*-block Dopants**		**Electronegativity**	**Bader Charge**
	N	3.04	5.78
s^2p^3	**P**	2.19	5.39
	As	2.18	5.23
	O	3.44	6.88
s^2p^4	**Se**	2.58	6.63
	Te	2.55	6.48
	F	3.98	7.72
s^2p^5	**Cl**	3.16	7.59
	Br	2.96	7.49